Electronic Supplementary Material (ESI) for Journal of Materials Chemistry A.

Supporting Information: Slow surface diffusion on Cu substrates in Li metal batteries

Ingeborg Treu Røe and Sondre Kvalvåg Schnell*

Department of Materials Science and Engineering, Norwegian University of Science and Technology, NTNU, Trondheim, Norway

E-mail: sondre.k.schnell@ntnu.no

Density Functional Theory Simulations

The surface diffusion barriers (SDBs) were calculated using the density functional theory (DFT) code Vienna *Ab intio* Simulation Package (VASP)[S1,S2] together with the climbing image Nudged Elastic Band (c-NEB) method.[S3–S6] The Li_sv and Cu_pv projector augmented wave pseudopotentials[S7] were expanded to energy cutoffs of 500 eV for the pure Li simulation cells, and 550 eV for the pure Cu as well as the combined Cu-Li simulation cells. The PBEsol functional[S8] was used. The lattice constants of the various Li crystal structures were tested previously,[S9] but the lattice constant of bulk Cu fcc was calculated to 3.55 Å, which is in agreement with the experimental lattice constant at 3.60 Å[S10] and the lattice constant of the materials project at 3.62 Å.[S11] The surface relaxation and c-NEB calculations were performed on simulation cells exposing the (001) and (111) fcc facets with dimensions exceeding 14 Å in all directions, plus a vacuum of more than 15 Å in the z-direction (normal to the surface). The Li-Cu simulation cell was created using a Cu fcc(001) simulation cell, and inserting Li atoms in all fcc(001) hollow sites to make the Li surface. To create 3.13% and 6.25% ratio of vacancies, 1 and 2 Li atoms were removed from the surface, respectively. The 43.75% vacant surface (corresponding to a uniform strain of less than 3%) was created by expanding 3x3 unit cells of Li fcc(001) to the 4x4 Cu fcc(001) substrate. The four uppermost layers of atoms in the z-direction of the simulation cells were free, while the rest of the atoms were fixed in space to mimic the bulk. The required number of bulk layers in the z-direction to achieve a stable surface was tested in figure S1, where the x-axis describe the height of the surface above the lowest bulk layer. Layer 1-4 are the four uppermost, free layers. Layer 1 is the first (*i.e.* the lowest) layer, and layer 4 the last (*i.e.* the highest). Although layer 4 still show some instability at 15 Å height, the remaining layers are stable, and the z-dimension of 14 Å was chosen to reduce the computational cost. All bulk and surface cells were relaxed to within 0.001 eV/Å. c-NEB was performed on five images for each surface diffusion path, and the max force on each of the images was relaxed to within 0.01 eV/Å.

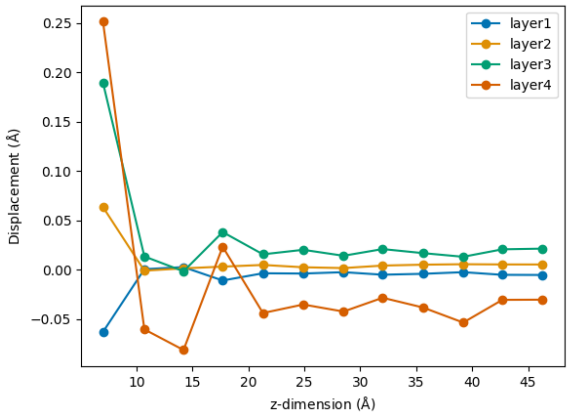

Figure S1: Change in atomic position relative to an ideal bulk position for the four uppermost layers in a Cu simulation cell. The count of the layers start from the bottom (i.e. layer 4 is the surface layer). The z-dimension describes the distance between the lowest bulk layer and the surface layer.

Molecular Dynamics Simulations

Melting Point Simulations

The melting points of Li and Cu were investigated to evaluate the accuracy of the Li and Cu MEAM-potentials.[S12] The calculations were performed using the NPT-ensemble with a Nose-Hoover thermostat and barostat[S13] on simulations cells containing 500 particles, and with periodic boundary conditions. The pressure was kept constant at 1 bar for all calculations, while the temperature was increased stepwise. At each temperature step, the simulation cell was allowed to equilibrate for 10 ns, before volume data was produced for 0.1 ns. Volume data was sampled blockwise every 0.01 ns during the production run. Every block consisted of 1000 volume samples from the last 0.001 ns before the block sampling point. These sample points were averaged to give a block volume. Lastly, all the block volumes were averaged to give the volume of the simulation cell at that temperature. Subsequently, the temperature was increased to the next step and the procedure repeated. The volume of the Cu cell was simulated at temperatures between 1200 K and 2100 K, and temperature steps of 20 K from

1500 K to 1800. The Li melting point was investigated for temperatures between 200 K and 700 K, with 20 K temperature steps from 250 K to 500 K.

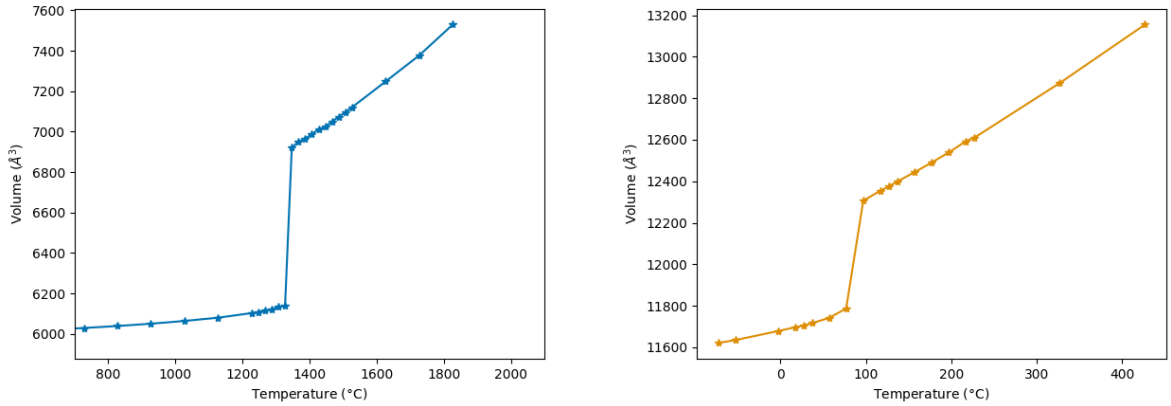

(a) (b)

Figure S2: Melting point calculations of (a) Cu and (b) Li using the MEAM potentials.

Lattice Constant Calculations

The lattice constants of Li and Cu predicted by the MEAM potentials were found using static runs with the damped dynamic minimization method[S14] in LAMMPS on simulation cells with 4000 particles and periodic boundary conditions. The energies of the Li and Cu simulation cells as a function of the lattice constant are shown in figure S3.

Surface Crystal Structure

The MD simulations of the Li and Cu-Li cells were performed in the canonical (NVT) ensemble with the Nose-Hoover thermostat for temperatures of 10 K, 50 K, 150K and 300 K on Cu-Li and Li simulation cells containing 4000 and 4400 particles, respectively, initialised in the fcc (001) structure. Periodic boundary conditions were used in all directions, and an initial vacuum exceeding 140 Å was added in the z-direction (normal to the surface). The simulation cells were relaxed using the damped dynamics minimization method,[S14] equilibrated for 0.01 ns with 0.01 ps thermostat relaxing time, and then ran for 1 ns with

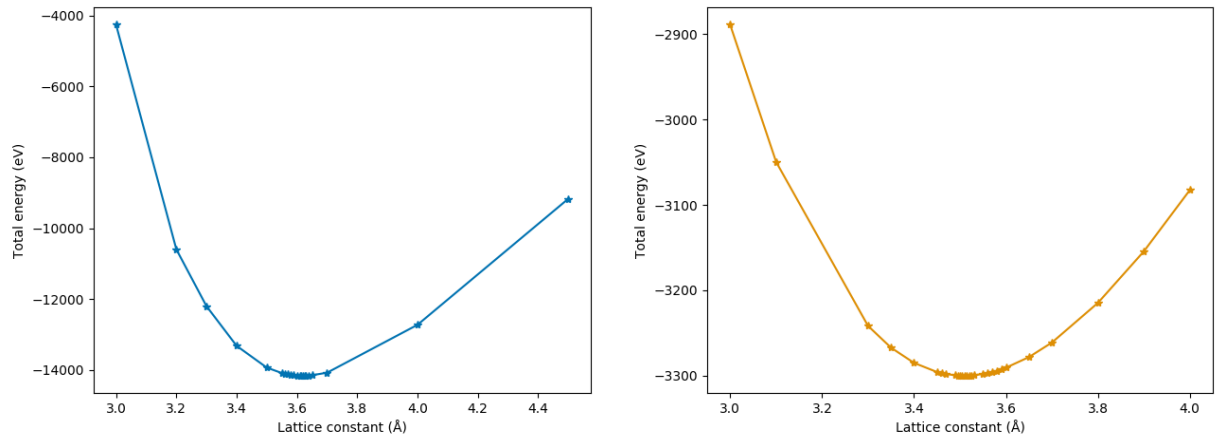

Figure S3: Total energy as a function of the lattice parameter of (a) Cu and (b) Li using the MEAM potentials.

0.1 ps thermostat relaxing time. Position data was sampled every 0.1 ps and 1 ps for the equilibration and run. The surface adaptive common neighbour analysis (sa-CNA) developed for this work was performed on the position data.

Figure S4 shows the weighted number of particles in a crystal structure (*i.e.* the ratio of atoms in the crystal structure over the total amount of surface atoms) of a Li surface on a clean Li substrate at 10 K, 50 K, 150 K, 200 K, 250 K and 300 K. We see that the initial fcc(001) is completely retained for temperatures up to 150 K, and retained for the majority of the surface atoms for temperatures up to 200 K.

Surface Adaptive Common Neighbour Analysis

About the sa-CNA

The *surface adaptive common neighbour analysis*[1] (sa-CNA) developed for binary surfaces in this work is based on the a-CNA code from Ovito,[S15,S16] which analyses single-element bulk structures. The regular a-CNA method detects the local crystal structure of a particle from the topology of the bonds connecting the nearest neighbours. The nearest neighbours are

[1]The code is available from: `https://github.com/sondresc/sa-CNA`

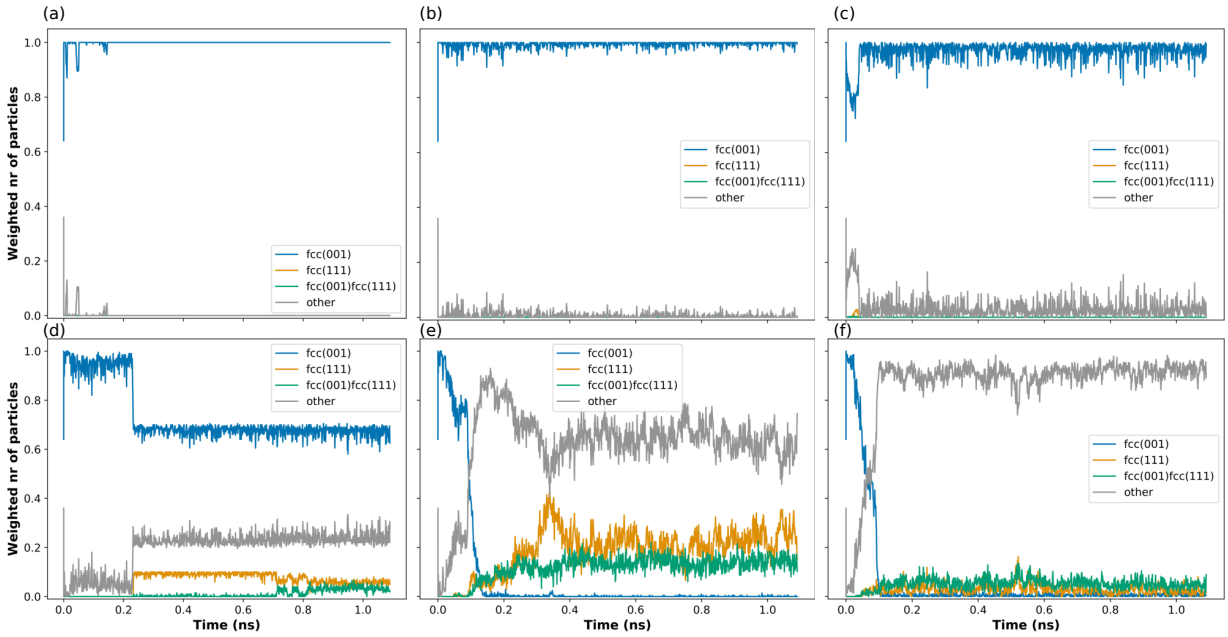

Figure S4: Crystal structure of the Li surface atoms on a Li substrate at (a) 10 K, (b) 50 K, (c) 150 K, (d) 200 K, (e) 250 K and (f) 300 K. The weighted number of particles is the ratio of particles in a crystal structure over the total amount of surface particles.

defined as all particles within a cutoff distance, r_{cut}, of the central particle. These particles are said to be bonded. In the a-CNA (as opposed to CNA), the cutoff distance is set locally for every particle. That is, the distance between the central particle and N_{max} nearest neighbours is averaged to find the local cutoff distance. For the close-packed fcc and hcp crystal structures, $N_{max}^{fcc} = 12$, and the cutoff is given by:

$$r_{cut,fcc}^{local} = \frac{1+\sqrt{2}}{2} \frac{\sum_{j=1}^{12} r_j}{12} \tag{S1}$$

where r_j is the distance between the central particle and the j^{th} nearest neighbour. Here, the cutoff distance is set between the first and the second neighbour shell, but for the bcc crystal structure, both shells are included. Thus, $N_{max}^{bcc} = 14$, and the expression for the local cutoff must account for the different distance to the two shells;

$$r_{cut,bcc}^{local} = \frac{1+\sqrt{2}}{2} \left[\frac{2}{\sqrt{3}} \frac{\sum_{j=1}^{8} r_j}{8} + \frac{\sum_{j=9}^{14} r_j}{6} \right] \tag{S2}$$

r_{cut}^{local} is now used to find the nearest neighbours, and for each central particle-nearest neighbour (cp-nn) pair three identifiers are used to describe the local crystal structure;

n_{cn} - Number of neighbouring particles the cp-nn pair has in common

n_b - Total number of bonds between the common neighbours

n_{lcb} - Number of bonds in the longest chain of bonds connecting the common neighbours

The identifiers are compared to the signature of the ideal crystal structures, which are found in table S1 and illustrated for the fcc and bcc (monoatomic, bulk) crystal structures in figure S5. Since the expression for $r_{cut,fcc}^{local}$ and $r_{cut,bcc}^{local}$ are different, the identifiers can only be compared to the signature of the crystal structure for which r_{cut}^{local} was calculated. Thus, finding the local crystal structure is an iterative process where the identifiers are calculated and matched to one target crystal structure at a time.

Table S1: The CNA signatures of the fcc, hcp and bcc crystal structures. N_{max} **is the maximum number of nearest neighbours allowed for the crystal structure.** N_{ID} **is the number of central particle-near neighbour pairs that match the specific CNA signature in the ideal crystal structure.**

Crystal structure	N_{max}	(n_{cn},n_b,n_{lcb})	N_{ID}
fcc	12	(4,2,1)	12
hcp	12	(4,2,1)	6
		(4,2,2)	6
bcc	14	(6,6,6)	8
		(4,4,4)	6

The sa-CNA method uses the same iteration to find local cutoff distance and structure identifiers to match against target crystal structures, but is modified to handle binary systems with AA-terminated surfaces as exemplified in figure S6. Therefore, two identifiers are added to the original three to describe the particle type of the central particle, t_{cp}, and its nearest neighbour, t_{np}. Notice that for the convenience of the code, the n_{lcb} identifier is split in two - n_{lmin} and n_{lmax} describing the minimum and maximum number of bonds a common neighbour possesses. As an example, the bulk fcc structure in figure S5(a) gets a CNA signature (n_{cn},n_b,n_{lmax},n_{lmin},t_{cp},t_{np}) = (4,2,1,1), while the bulk bcc structure in figure S5(b) gets (n_{cn},n_b,n_{lmax},n_{lmin},t_{cp},t_{np}) = (4,4,2,2). Furthermore, the max amount of neighbours

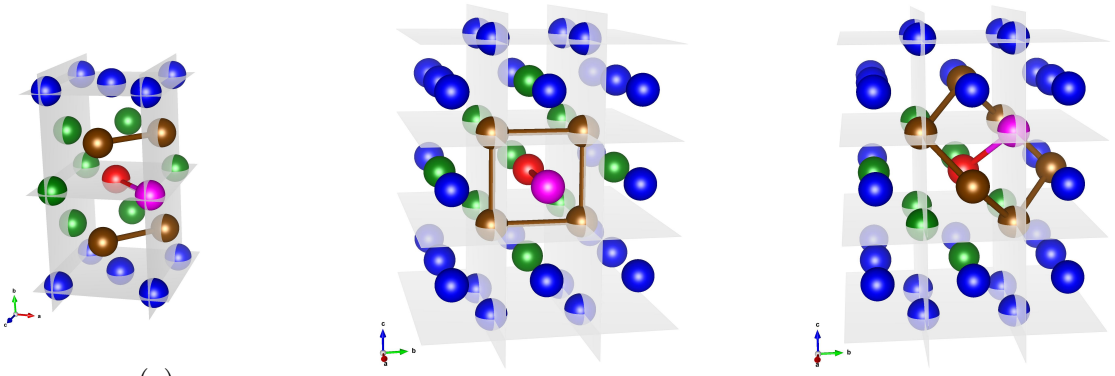

(a) (b) (c)

Figure S5: Illustrations of the CNA identifiers for (a) fcc, (b) bcc with CNA signature (4,4,4) and (c) bcc with CNA signature (6,6,6). The different types of particles are shown in colours; central particle in red, near neighbour (in question) in purple, common neighbours in brown and the remaining near neighbours in green. Particles in the next neighbour shell are coloured blue. Grey planes shows the unit cell.

are different for the surface structures than the corresponding bulk structure, rendering different signatures for the surface structures. An overview of the signatures developed for the purpose of this work is found in table S2. A selection of the CNA signatures for the different geometries is also shown in figure S7. For the fcc(001), fcc(111) and bcc(001) geometries, the same rules as for conventional (bulk) a-CNA are followed, and the signature is well defined. However, the fcc(001)fcc(111) geometry is less well defined, and the aid of MD simulation data has been used together with the usual crystallographic data to find the CNA signature.

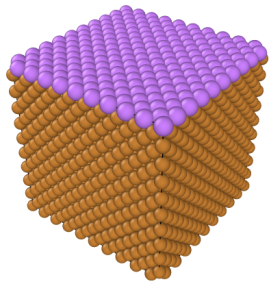

Figure S6: Example of a binary surface with AA-termination. The bulk consists of one particle type (brown), and the surface of the other (purple).

Table S2: CNA signatures for the fcc(001), fcc(111), fcc(001)fcc(111) and bcc(001) geometries used in the sa-CNA for binary surfaces.

Crystal structure	N_{max}	(n_{cn},n_b,n_{lmax},n_{lmin},t_{cp},t_{np})	N_{ID}
fcc(001)[a]	8	(4,1,1,1,2,2)	4
		(4,2,1,1,2,1)	4
fcc(111)[b]	9	(3,1,1,0,2,2)	6
		(4,2,1,1,2,1)	3
fcc(001)fcc(111)[c]	10	(4,3,2,1,2,2)	2
		(3,1,1,0,2,2)	2
		(3,1,1,0,2,2)	4
		(4,3,2,1,2,1)	2
		(4,2,1,1,2,1)	1
		(3,0,0,0,2,1)	1
bcc(001)[d]	9	(2,1,1,1,2,2)	4
		(5,4,2,1,2,1)	4
		(4,4,2,2,2,1)	1

[a] Bulk fcc (001) with one surface layer in fcc (001)
[b] Bulk fcc (111) with one surface layer in fcc (111)
[c] Bulk fcc (001) with one surface layer in fcc (111)
[d] Bulk bcc (001) with one surface layer in bcc (001)

Testing of the sa-CNA analysis

Test cases for the sa-CNA analysis were set up using the Lennard-Jones potential in LAMMPS with a cutoff of 7 Å. Two types of particles were defined; type 1 always constituted the bulk and type 2 made up the surface, and arranged in three different geometries; fcc(001) where bulk and surface share fcc(001) crystal structure, fcc(111) where bulk and surface share

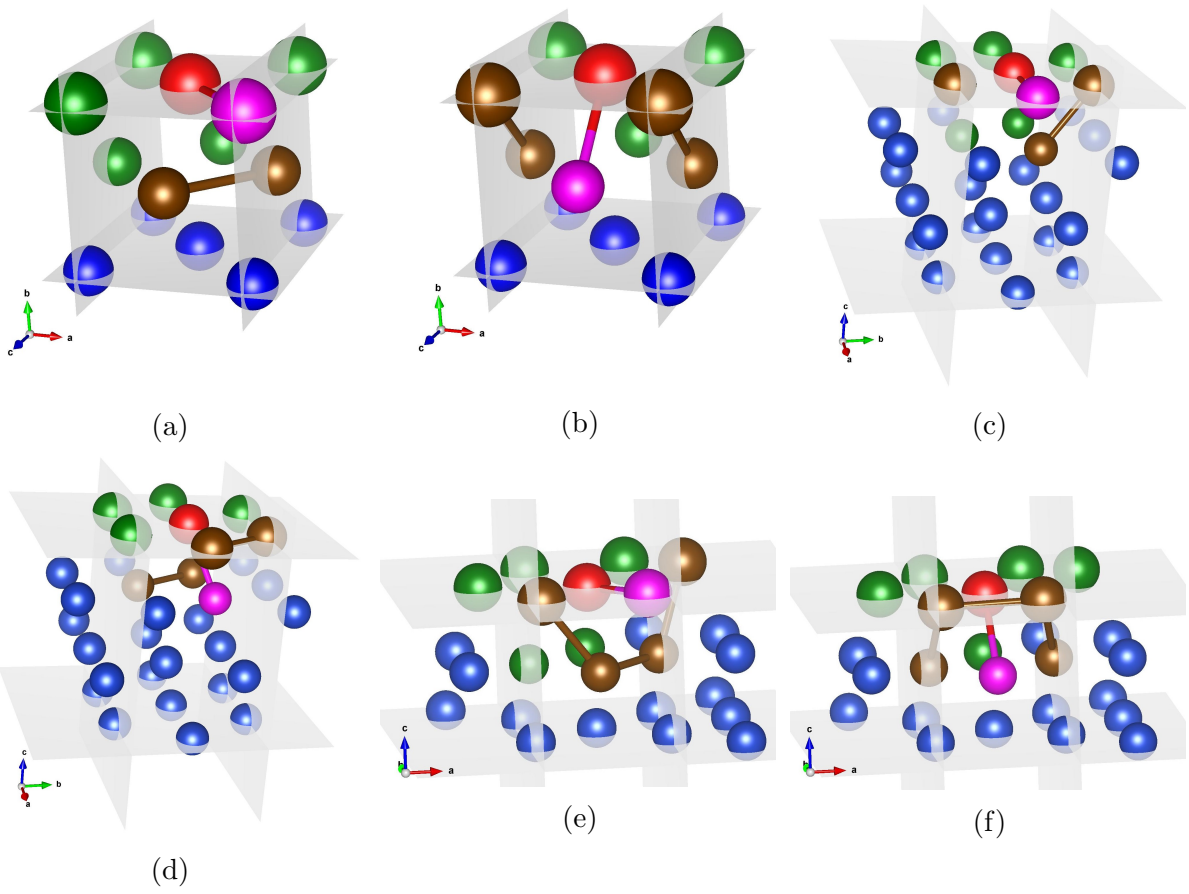

Figure S7: Illustrations of the CNA identifiers for surfaces; (a) fcc(001) with CNA signature (2,1,1,1,2,2), (b) fcc(001) with CNA signature (4,2,1,1,2,1), (c) fcc(111) with CNA signature (3,1,1,0,2,2), (d) fcc(111) with CNA signature (4,2,1,1,2,1), (e) fcc(001)fcc(111) with CNA signature (4,3,2,1,2,2) and (f) fcc(001)fcc(111) with CNA signature (4,3,2,1,2,1). The different types of particles are shown in colours; central particle in red, near neighbour (in question) in purple, common neighbours in brown and the remaining near neighbours in green. Particles in the next neighbour shell are coloured blue. Grey planes shows the unit cell.

fcc(111) crystal structure, and fcc(001)fcc(111) where bulk has fcc(001) and surface has fcc(111) crystal structure. Epsilon and sigma values for type 1-type 1 interaction were 2.0 eV and 2.3 Å for all three geometries. For type 2-type 2 interaction, epsilon and sigma were the same as for type 1 except for fcc(001)fcc(111) where epilon was 2.5 eV. Epsilon for the type 1-type 2 interaction was always defined to 50 % of the type 1-type 1 interaction (i.e. 1 eV), while sigma remained 2.3 Å. An overview of the different Lennard-Jones parameters is found in table S3.

Table S3: Lennard-Jones parameters for the three test cases for the sa-CNA.

Interaction	Epsilon (eV)		Sigma (Å)
	fcc(001) & fcc(111)	fcc(001)fcc(111)	All
Type 1	2.0	2.0	2.3
Type 2	2.0	2.5	2.3
Type 1-2	1.0	1.0	2.3

The geometries consisted of around 600 particles, of which around 50 particles were placed on the surface (type 2 particles). MD simulations were run in the NVT ensemble with a Nose-Hoover thermostat[S13] for temperatures of 10 K, 50 K, 100 K, 150 K, 200 K and 250 K for all of the geometries to test the sensitivity of the code to thermal vibrations. The simulation cells were first relaxed using the damped dynamics minimization method,[S14] initialized with 0.0001 ps timesteps and 0.01 ps thermostat relaxing time for 0.1 ps, and then ran for 0.1 ns with 0.001 ps timesteps and 0.1 ps thermostat relaxing time. The particle positions were sampled every 0.01 ps during the initialization, and every 0.001 ns during the run. The ratio of surface particles detected in different structures over the total amount of surface particles as a function of time was tracked and is displayed in table S8. The initialization of the geometries is included in the curves, which is why the first 0.0001 ns is unstable as the temperature is rising to the set temperature in this region and the geometry is approaching equilibrium. As seen in all the subfigures, the initial geometries do not match the intended crystal structure. This is due to the set-up of the geometries in LAMMPS rather than the a-CNA analysis. However, the weighted particle number stabilizes after that

for all the temperatures, meaning that the analysis is stable and relatively insensitive to (small) thermal vibrations.

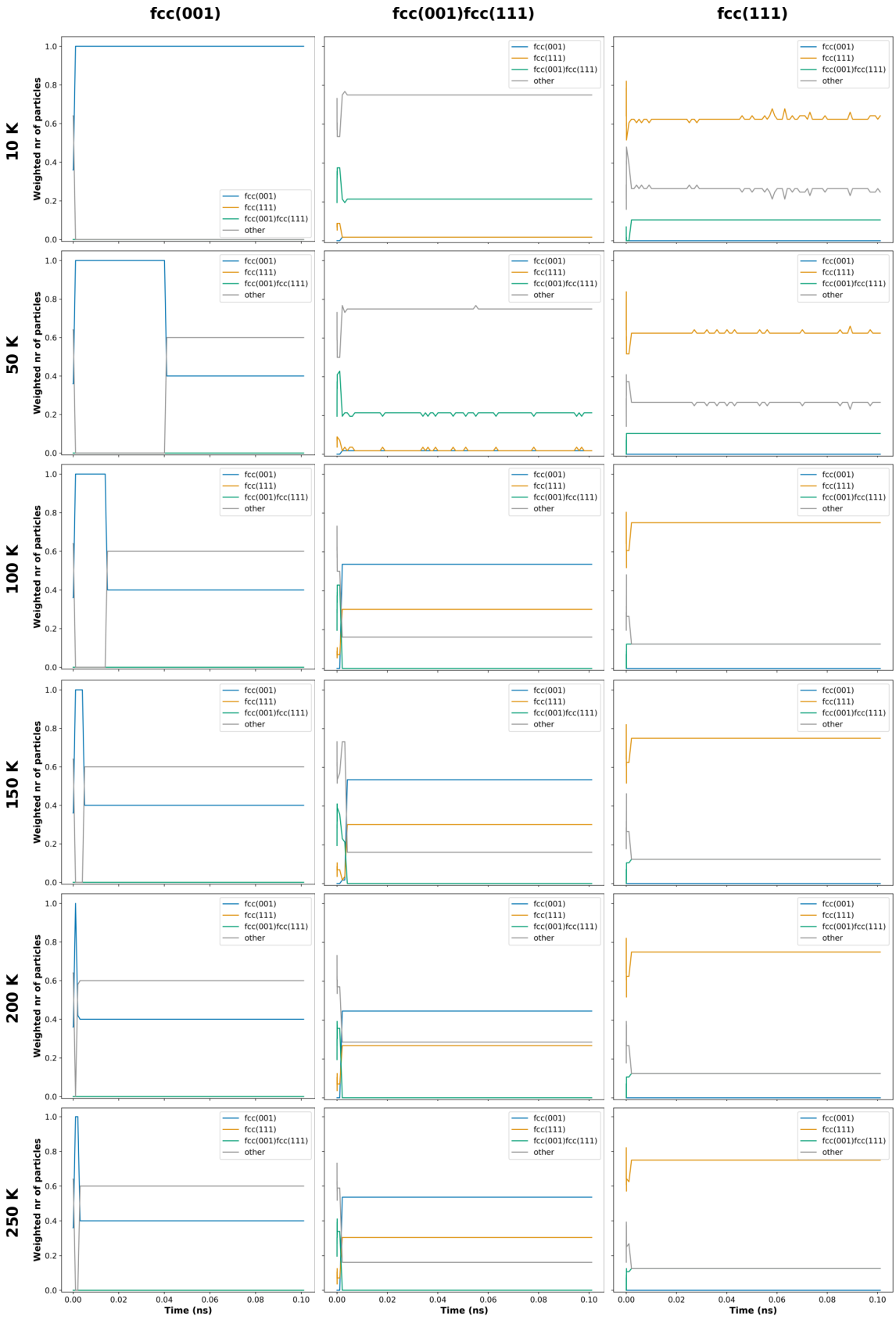

Figure S8: The ratio of surfaces particles detected in a crystal structure over the total amount of surface particles as a function of time for the three geometries.

References

(S1) Kresse, G.; Furthmüller, J. Efficiency of ab-initio total energy calculations for metals and semiconductors using a plane-wave basis set. *Computational Materials Science* **1996**, *6*, 15–50.

(S2) Kresse, G.; Joubert, D. From ultrasoft pseudopotentials to the projector augmented-wave method. *Physical Review B* **1999**, *59*, 1758–1775.

(S3) Jonsson, H.; Mills, G.; Jacobsen, K. W. Nudged elastic band method for finding minimum energy paths of transitions. *Classical and Quantum Dynamics in Condensed Phase Simulations - Proceedings of the International School of Physics* **1998**, 385–404.

(S4) Henkelman, G.; Uberuaga, B. P.; Jónsson, H.; Jó, H. A climbing image nudged elastic band method for finding saddle points and minimum energy paths. *The Journal of Chemical Physics* **2000**, *113*, 214106.

(S5) Henkelman, G.; Jónsson, H. Improved tangent estimate in the nudged elastic band method for finding minimum energy paths and saddle points. *Journal of Chemical Physics* **2000**, *113*, 9978.

(S6) Sheppard, D.; Xiao, P.; Chemelewski, W.; Johnson, D. D.; Henkelman, G. A generalized solid-state nudged elastic band method. *The Journal of Chemical Physics* **2012**, *136*, 74103.

(S7) Blöchl, P. E. Projector augmented-wave method. *Physical Review B* **1994**, *50*, 17953.

(S8) Perdew, J. P.; Ruzsinszky, A.; Csonka, G. I.; Vydrov, O. A.; Scuseria, G. E.; Constantin, L. A.; Zhou, X.; Burke, K. Restoring the Density-Gradient Expansion for Exchange in Solids and Surfaces. *Physical Review Letters* **2008**, *100*, 136406.

(S9) Røe, I. T.; Selbach, S. M.; Schnell, S. K. Crystal Structure Influences Migration along Li and Mg Surfaces. *Journal of Physical Chemistry Letters* **2020**, *11*, 2891–2895.

(S10) Davey, H. P. Precision measurements og the lattice constants of twelve common metals. *Phys. Rev* **1925**, *25*, 753–761.

(S11) Jain, A.; Ong, S. P.; Hautier, G.; Chen, W.; Richards, W. D.; Dacek, S.; Cholia, S.; Gunter, D.; Skinner, D.; Ceder, G.; Persson, K. A. Commentary: The materials project: A materials genome approach to accelerating materials innovation. *APL Materials* **2013**, *1*, 011002.

(S12) Baskes, M. I. Modified embedded-atom potentials for cubic materials and impurities. *Physical Review B* **1992**, *46*, 2727–2742.

(S13) Hoover, W. G. Canonical dynamics: Equilibrium phase-space distributions. *Physical Review A* **1985**, *31*, 1695–1697.

(S14) Sheppard, D.; Terrell, R.; Henkelman, G. Optimization methods for finding minimum energy paths. *Journal of Chemical Physics* **2008**, *128*, 134106–.

(S15) Stukowski, A. Structure identification methods for atomistic simulations of crystalline materials. *Modelling and Simulation in Materials Science and Engineering* **2012**, *20*, 045021.

(S16) Stukowski, A. Visualization and analysis of atomistic simulation data with OVITO–the Open Visualization Tool. *Modelling and Simulation in Materials Science and Engineering* **2010**, *18*, 015012.